Research Article Vol. 30, No. 2 / 17 Jan 2022 / Optics Express 1388
Optics EXPRESS

# Multiplexed Mach-Zehnder interferometer assisted ring resonator sensor

MUKESH YADAV* AND ASTRID AKSNES

*Department of Electronic Systems, Norwegian University of Science and Technology (NTNU), Trondheim NO- 7491, Norway*
*mukesh.yadav@ntnu.no

**Abstract:** A Mach-Zehnder interferometer assisted ring resonator configuration (MARC)-based multiplexed photonic sensor with a large measurement range is experimentally demonstrated. The presented MARC sensor consists of a balanced Mach-Zehnder interferometer and a ring resonator acting as a sensing component. It produces transmission responses with unique spectral signatures, which depend on the physical angular separation between the through port and the drop port waveguides. These unique spectral signatures enhance the effective free spectral range of ring resonators. Hence MARC sensors with a large measurement range are realized. We experimentally demonstrated that the measurement range from the MARC with 135° angular separation is 8x larger than a standard ring resonator. Moreover, by utilizing the MARC, we distinguished the responses from two and three ring resonators multiplexed together. These results verify proof-of-principle for the MARC-based sensors. This inexpensive compact multipurpose device holds promise for numerous applications.



## 1. Introduction

Silicon-on-insulator (SOI) based optical waveguide sensors have been intensively investigated for medical diagnosis, food quality control, environmental monitoring, and other applications. These sensors utilize optical waveguide-based transducers for transforming the surrounding refractive index change due to target analytes into a measurable change in the transmission. There exist several types of transducers that use various kind of techniques to transform the refractive index change into the transmission change. Ring resonators [1–4], Mach-Zehnder interferometers [5,6], Bragg gratings [7,8], cascaded micro-ring resonators [9], and cascaded Mach-Zehnder interferometer and ring resonator [10,11] are a few examples of optical waveguide-based transducers. Among these transducers, ring resonators are considered as one of the most promising for refractive index sensing as they can be made small and resonance shifts observed from resonators can be tracked easily with high accuracy. Sensors with small footprint are highly desirable in sensing applications as they reduce the amount of sample volume required during detection. High accuracy increases the detection limit of the sensor and for ring resonator sensors it is achieved by increasing the Q-factor. In standard ring resonators, high Q-factor is attained by reducing the optical bending loss along the ring, which is achieved by changing the dimension of the waveguide and increasing the ring radius [12]. This method improves the Q-factor but shortens the free spectral range, which consequently limits the measurement range. Thus, realization of a ring resonator sensor with high Q-factor, wide measurement range and small footprint is challenging. Moreover, short measurement range also limits the multiplexing capability of ring resonators. Multiplexing is advantageous in enhancing the throughput, which consequently reduces the overall cost of the device. In addition to high throughput, it also provides flexibility of placing a reference sensor in close proximity to the actual sensor for drift correction and control experiments. To overcome the challenge of short measurement range, real-time continuous tracking of resonance is required. This is generally achieved by tracking the resonance with faster rate than the analyte binding rate. However, tracking of resonance with

#448023 https://doi.org/10.1364/OE.448023
Journal © 2022 Received 9 Nov 2021; revised 18 Dec 2021; accepted 24 Dec 2021; published 4 Jan 2022

Optics EXPRESS

faster rate normally requires an expensive tunable laser source with fast scanning speed and this solution could be ineffective for bulk sensing, where the refractive index change is abrupt. In general, multiplexing in ring resonator-based sensors is addressed by fabricating multiple ring resonator sensors in a parallel configuration. Ring resonators fabricated in parallel configurations increase the chip size and typically require multiple photodetectors or photodiode arrays [4,13].

Recently, we presented a Mach-Zehnder interferometer assisted ring resonator configuration (MARC) that generates unique spectral signatures by tuning the angular separation between the through port and the drop port waveguides [14]. Spectral signatures generated from the MARC enhance the effective free spectral range of ring resonators. In this paper, we present a novel MARC sensor that can simultaneously provide both large measurement range and multiplexing capability. Moreover, these improvements are achieved without compromising the Q-factor or the detection limit provided by the ring resonator.

## 2. Theory

A MARC is a design consisting of a balanced Mach-Zehnder interferometer (MZI) and an add-drop ring resonator (RR). The phase response at the ring resonator drop port is engineered by physically changing the angular separation between the drop port and the through port waveguides. The tailored phase response is converted into the transmission response by utilizing a balanced MZI. The transmission spectra obtained from MARC with specific angular separation show unique spectral signatures with large effective free spectral ranges [14].

Figure 1 shows the schematic of a MARC sensor comprised of a single RR with the ring radius of R1 and the angular separation of $\theta$ radians. As we presented in our earlier work, an angular separation of $\theta$ radians results in a phase response at the drop port with $\theta$ radians phase accumulation between resonances. This angular separation dependent phase response is translated into an intensity response with the MZI and shows unique spectral signatures. As illustrated in Fig. 1, the whole MARC device is covered with cladding except the ring resonator. The uncladded ring resonator acts as a sensing element and produces resonance wavelength shifts as a function of the refractive index change in the surrounding. The resonance shift caused by the refractive index change is observed at the through port output and the MARC output. MARC sensors with specific ring radius and angular separation can be designed to enhance the effective free spectral range of ring resonators without compromising the Q-factor.

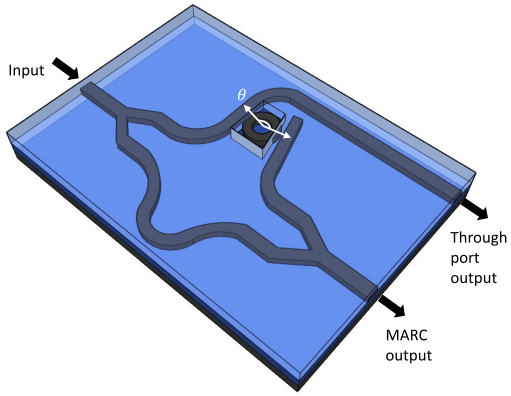


**Fig. 1.** Schematic of a MARC sensor with an uncladded ring resonator with ring radius of r and angular separation between through port and drop port waveguides of $\theta$.

Optics EXPRESS

Through port and MARC transmission responses are given as:

$$T_{\text{through}} = \frac{\gamma_1^2 + \gamma_2^2 a^2 - 2a\gamma_1\gamma_2 \cos\psi}{1 + \gamma_1^2\gamma_2^2 a^2 - 2a\gamma_1\gamma_2 \cos\psi}, \tag{1}$$

$$T_{\text{MARC}} = \frac{1}{4}[1 + |t|^2 + 2|t| \cos\phi], \tag{2}$$

where, $\phi$ is the phase response at the drop port, $\psi$ is the round-trip phase shift, $\gamma_1(\gamma_2)$ is the self-coupling coefficient of the coupler and $a$ is the round-trip amplitude transmission factor between the input and output couplers. $t$ is the drop port amplitude transmission response and it is given as, $t = -\frac{\sqrt{1-\gamma_1^2}+\sqrt{1-\gamma_2^2}a_d \exp[i(\psi \frac{\theta}{2\pi})]}{1-\gamma_1\gamma_2 a \exp[i(\psi)]}$. $\theta$ in the phase term is the angular separation between the through port and the drop port waveguides.

Any refractive index change in the surrounding of the ring resonator results in a resonance shift. Resonance shifts are proportional to the refractive index change and can be measured from both through port output and the MARC output. Resonance shifts measured from both outputs are similar. However, shifts measured from the through port output are more accurate than the MARC output. It is because the through port output provides resonances with higher Q-factor than the MARC output. The resonance shift as a function of refractive index change obtained from the through port output and the MARC output is given by [3],

$$S = \frac{\Delta\lambda}{\Delta n} = \frac{m}{L}\left(\frac{\partial n_{eff}}{\partial n_{bulk}}\right)^{-1}, \tag{3}$$

where, $L$ is the round-trip length, m is the cavity mode order, $n_{bulk}$ is the bulk refractive index due to the analyte and $n_{eff}$ is the effective refractive index of the guided mode.

In addition to the sensitivity, one of the most important parameters of a sensor is the measurement range, which defines its usability and versatility. For the case of the MARC sensor, the measurement ranges of the through port output and the MARC output are not identical. The measurement ranges of the through port and MARC outputs are given by,

$$\Delta n_{max}^{through} = \frac{FSR}{S}, \tag{4}$$

$$\Delta n_{max}^{MARC} = \frac{FSR_e}{S}, \tag{5}$$

where, $\Delta n_{max}$ is the maximum detectable refractive index and $FSR$ is the free spectral range of the ring resonator given by $\frac{\lambda^2}{n_g 2\pi r}$, where $n_g$ is the group index, $\lambda$ is the vacuum wavelength and $r$ is the ring radius. $FSR_e$ is the effective free spectral range of the MARC output and is an integer multiple of $FSR$ ($FSR_e = N \cdot FSR$). The integer multiple, N, depends on the angular separation between the drop port and the through port waveguides. This is explained in detail in our previous work [14].

As shown in Eq. (4), the measurement range of the through port output is limited by the free spectral range. In contrast to the through port response, the MARC output provides a measurement range that is only partially limited by the free spectral range and can be enhanced by changing the angular separation. Figure 2 illustrates the difference between the measurement range obtained from the through port output and the MARC output, and shows the MARC enhancement of the the measurement range.

Moreover, sensors with large measurement ranges are best suited for multiplexing. For the case of the standard ring resonator sensor, the measurement range depends on the free spectral range, and can be increased by reducing the ring radius. However, a decrease in the ring radius reduces the Q-factor of the ring resonator. In contrast, the MARC sensor with a specific angular

Optics EXPRESS

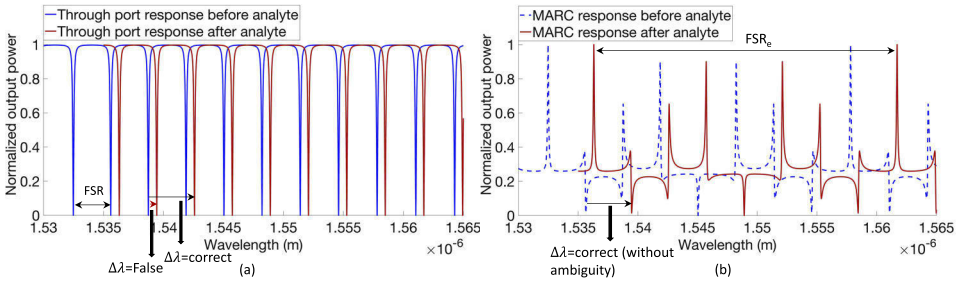


**Fig. 2.** . (a) Resonance shift measurement using the through port output (standard ring resonator), (b) Resonance shift measurement using the MARC output. The transmission response obtained from the through port output presents a case of false positive when the shift is abrupt and larger than the FSR.

separation can enhance the effective free spectral range of the ring resonator without affecting the Q-factor and can also produce a transmission response with a unique spectral signature. These two features of a MARC can be utilized for multiplexed sensing when distinct rings with varying angular separations are integrated with a balanced Mach-Zehnder interferometer. Figure 3(a) and Fig. 3(b) show the multiplexing of 2 and 3 ring resonators, respectively. For the case of the MARC with 2 rings, a balanced MZI is integrated with 2 ring resonators with different ring radius and angular separations. Rings with different angular separations are used to tag both rings with distinct spectral signatures, which allows easier tracking of resonance shifts for both resonators. Different ring radius reduces the number of overlapping resonances from both rings over a narrow wavelength range.

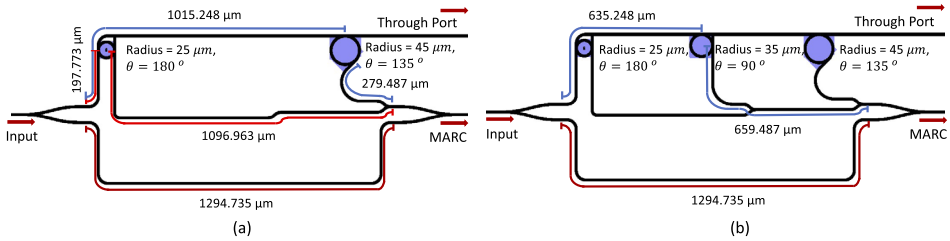


**Fig. 3.** (a) Schematic of MARC with 2 ring resonators with 180° and 135° angular separation. Radii for these two rings are 25 $\mu$m and 45 $\mu$m, respectively. (b) Schematic of MARC with 3 ring resonators. For this case, an additional ring resonator with 35 $\mu$m ring radius and 90° is integrated with the MARC.

## 3. Sensor design and fabrication

MARC sensors were designed with silicon strip waveguides, supporting the fundamental TE-like mode at 1550 nm wavelength. Strip waveguides were 500 nm wide and 220 nm high. MARC sensors consisting of a ring resonator with ring radius of 45 $\mu$m and angular separation of 135° were designed for measuring the sensitivity and the measurement range. Several MARC sensors were designed with two and three ring resonators. For the case of MARC with 2 ring resonators, two rings with ring radii of 25 $\mu$m and 45 $\mu$m, and angular separations of 180° and 135° were integrated into a balanced MZI. Similarly, for MARC sensors consisting of 3 ring resonators, a balanced MZI was integrated with three ring resonators with ring radii of 25 $\mu$m, 35 $\mu$m and 45 $\mu$m, and angular separations of 180°, 90° and 135°, respectively. Moreover, input and output

Optics EXPRESS

waveguides were designed with inverted tapered silicon waveguides to enhance the coupling efficiency. Inverted taper silicon waveguides were 300 $\mu$m long with starting width of 70 nm.

MARC sensors were fabricated on SOI wafers with 220 nm of hydrogenated amorphous silicon on top of the 1 $\mu$m thermal oxide layer. Amorphous silicon was deposited on a thermal oxide wafer by plasma enhanced chemical vapor deposition (PECVD) system using SiH4 and Ar gases. Silicon strip waveguides with 500 nm width were patterned by electron beam lithography (Elionix ELS-G100) using e-beam resist (Allresist AR-P 6200). Lithography was followed by dry etching using inductively coupled plasma reactive ion etching (ICP-RIE). SU8 polymer strips were photolithographically patterned on top of silicon inverted tapers. SU8 strips were 300 $\mu$m long, 2 $\mu$m wide and 2 $\mu$m high. The complete chip was covered with 400 nm layer of Polymethyl methacrylate (PMMA) and a small area over the ring resonators was exposed with electron beam lithography to ensure that only the ring resonator interacts with the refractive index change in the surrounding. For controlled flow of solution over each ring resonator in the MARC sensors, three 150 $\mu$m wide and 80 $\mu$m high microfluidic channels were made on Poly-Di-Methyl Siloxane (PDMS) polymer using soft lithography. For sensing experiments, PDMS microfluidics and the photonic chip were clamped together with an acrylic plate. Figure 4 presents the fabricated MARC sensor clamped with PDMS microfluidics. Note that this fabricated sensor design is suboptimal and only shows a proof-of-principle. Further work involves optimizing the quality factor and the angular separation.

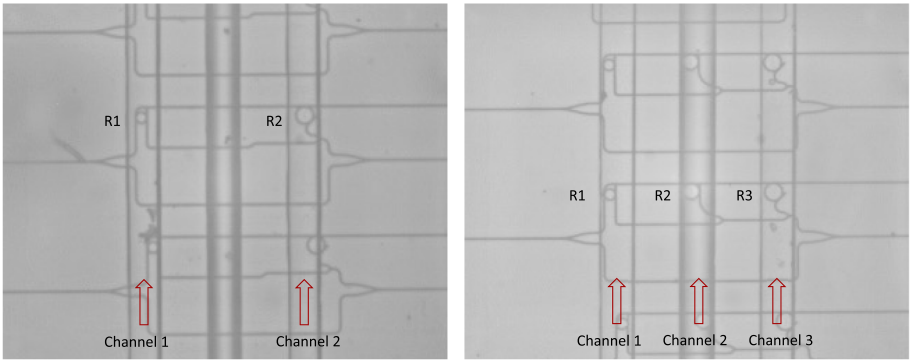


**Fig. 4.** (a) Fabricated MARC sensor with 2 ring resonators, (b) MARC sensor with 3 ring resonators with different radii and angular separations.

## 4. Experimental characterization

For experimental characterization, the photonic chip clamped with the PDMS microfluidics was placed on the translational stage. Solutions with analyte were pumped through the microfluidic channel with the syringe pump at 20 $\mu$l/min rate. A tapered lensed fiber with 14 $\mu$m working distance and 2.5 $\mu$m spot diameter was used to couple light into the waveguide from an external cavity laser (Thorlabs TLK-L1550M) with central wavelength of 1550 nm. A polarization controller (Thorlabs FPC562) was placed between the laser source and tapered fiber to control the polarization of the light from the laser source and to enhance the coupling to the TE-like mode of the waveguides. Two single mode optical fibers connected with InGaAs photodetectors (Thorlabs DET10C2) were placed at the output waveguides to capture the optical power from the through output and the MARC output. Figure 5 presents the transmission spectra obtained from the fabricated MARC with a single resonator with 135° angular separation and ring radius of 45 $\mu$m. The transmission response from the through port output presents the standard ring resonance response and shows a Q-factor of 10000 and free spectral range of ~2 nm. The transmission

Optics EXPRESS

response from the MARC output presents a unique spectrum consisting of non-identical adjacent resonances unlike the through port response. The effective free spectral range measured from the MARC output was ~16.1 nm, which is 8 times larger than the conventional free spectral range measured from the through port. The measurement range of a ring resonator based-refractive index sensor, the maximum refractive index change that can be detected, is dependent on the free spectral range and challenging to extend without affecting the Q-factor. The measured effective free spectral range from MARC provides larger measurement range to the sensor and without affecting the Q-factor. To analyze this property of the MARC sensor, refractive index sensing measurements were performed on the MARC using saline solutions with varying concentrations. Figure 5(a) shows the transmission spectra from the MARC for deionized water and saline solutions with 6%, 12% and 18% salt concentration. Linear relationship was observed between the resonance shift and saline solution concentration, as shown in Fig. 5(b). The MARC sensitivity was 80.4 pm/% salt and it was calculated from the linear fit of resonance shifts. The error bar in Fig. 5(b) is larger than expected. We believe that this is due to some salt crystallization on the waveguide sidewalls of the two sensors, which were exposed to saline solutions for several hours. The salt crystallization reduced the sensitivity of these two sensors and increased the error bar in the measured resonance shift. As shown in Fig. 5(a), the transmission response from the MARC output clearly shows that the measured shifts are much smaller than the effective free spectral range. The average resonance shift measured for 18% solution was 1.45 nm and it used 72% of the measurement range obtained from the through port output. In contrast this shift utilized only 9% percent of the measurement range provided by the MARC output. Note that during sensing experiments, no TEC controller was used to regulate the chip temperature. All measurements were performed at room temperature. Saline solutions were stored at room temperature.

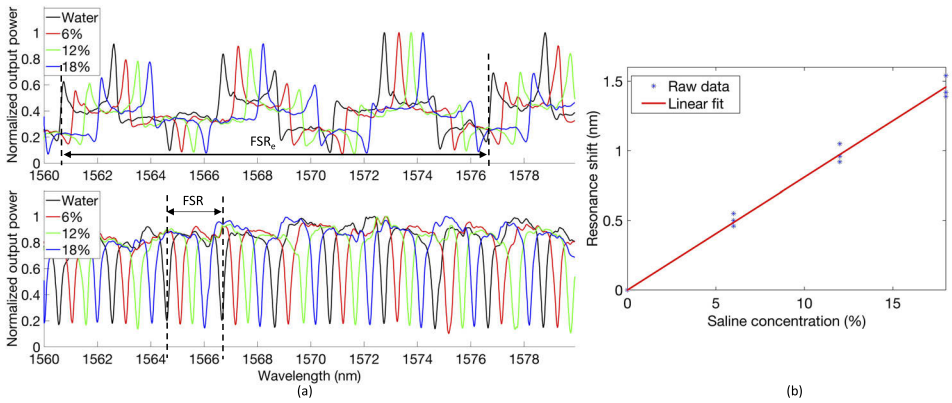


**Fig. 5.** (a) Transmission response obtained from MARC and through port outputs for different saline solutions, (b) Resonance shift for different saline solutions.

In this paper, in addition to the sensitivity and the measurement range, we also demonstrate the multiplexing capability of the MARC sensor. For the multiplexing experiment, two MARC sensor configurations were fabricated. In one configuration, the MARC sensor was designed to demonstrate multiplexing of two ring resonators. For this configuration, two ring resonators were integrated with a balanced MZI. The other configuration was designed with 3 ring resonators for multiplexing of 3 ring resonators. For the case of the MARC with 2 rings, the ring with 25 $\mu$m radius and 180° angular separation was used as a reference sensor and the ring with 45 $\mu$m radius and 135° angular separation was used for detecting varying saline concentrations. To improve the accuracy of the measured resonance shift, we measured both the through port output and the MARC output. From the through port output, we extracted precise information on the

Optics EXPRESS

resonance shift. Steps followed during the sensing experiment and corresponding measured resonance shifts are presented in Table 1. In step 1, deionized water was flowed over both rings (R1 and R2) to obtain the initial relative resonance shift between responses from both ring resonators. In steps 2-4, deionized water was continuously flowed over ring R1 and saline solutions with increasing concentrations were successively flowed over ring R2. For each saline solution, the relative resonance shift ($\Delta\lambda_{12}$) was measured. From measured relative resonance shifts and initial relative resonance shift, the effective resonance shift ($\Delta\lambda_{eff}$) for each saline solution was calculated and listed in Table 1. The resonance shifts obtained for different saline solutions show linear relationship, which is consistent with measurement results presented in the previous section. Figure 6(a) presents the transmission spectrum obtained from MARC with two rings when deionized water was flowed over both rings. Figure 6(b) shows the transmission obtained when 6% saline solution was flowed over the ring with 135° angular separation. The effective resonance shift was 0.52 nm. From the reference sensor with 180° angular separation, we measured ~20 pm shift after switching the saline solutions in the sensing channel. This shift is probably due to a small temperature difference between the two different solutions. To de-multiplex the responses of two rings from the combined MARC transmission, theoretically estimated responses for each ring were overlayed the combined response.

For the case of the MARC with 3 rings, the ring with 180° angular separation was used as the reference sensor and rings with 90° and 180° were utilized for sensing. Table 2 presents an overview of the sensing experiment performed on the MARC with 3 ring resonators. Resonance shifts from sensing rings when exposed to specific saline solution are listed in the table. Figure 6(c) shows the transmission response obtained when deionized water was flowed over all three rings. Like the MARC with 2 rings, the MARC transmission response was overlayed with theoretically estimated responses for each ring to easily de-multiplex the response from each sensor. Figure 6(d) shows the transmission response obtained when 18% saline solution was flowed over the ring with 135° angular separation and deionized water over the ring with the 90° angular separation. The corresponding resonance shift was 1.52 nm. The measurement results from the MARC with two and three rings clearly show that by combining several rings (with different angular separation and radius) with a balanced MZI allows easier multiplexing of ring resonator sensors. In addition, the reference sensor from the MARC with 2 rings and 3 rings showed a resonance shift of ~20 pm. This shift is less than 5% of the shift from the 6% saline solution, which shows that the set-up was stable without a TEC. However, the temperature stability of the set-up could be further improved by utilizing a TEC controller.

**Table 1. Overview of sensing experiments performed on the MARC with two ring resonators.**

| Steps | R1 (180°) | R2 (135°) | $\Delta\lambda_{12}$ | $\Delta\lambda_{eff}$ |
|---|---|---|---|---|
| 1 | water | water | 1.08 nm | |
| 2 | water | 6% | 1.6 nm | 0.52 nm |
| 3 | water | 12% | 2.07 nm | 0.99 nm |
| 4 | water | 18% | 2.57 nm | 1.49 nm |

**Table 2. Overview of sensing experiments performed on the MARC with three ring resonators.**

| Steps | R1 (180°) | R2 (90°) | $\Delta\lambda_{12}$ | $\Delta\lambda_{eff}$ | R3 (135°) | $\Delta\lambda_{13}$ | $\Delta\lambda_{eff}$ |
|---|---|---|---|---|---|---|---|
| 1 | water | water | 1.05 nm | | water | 0.69 nm | |
| 2 | water | water | 1.05 nm | | 18% | 2.21 nm | 1.52 nm |
| 3 | water | 18% | 2.57 nm | 1.52 | 18% | 2.21 nm | 1.52 nm |

Optics EXPRESS

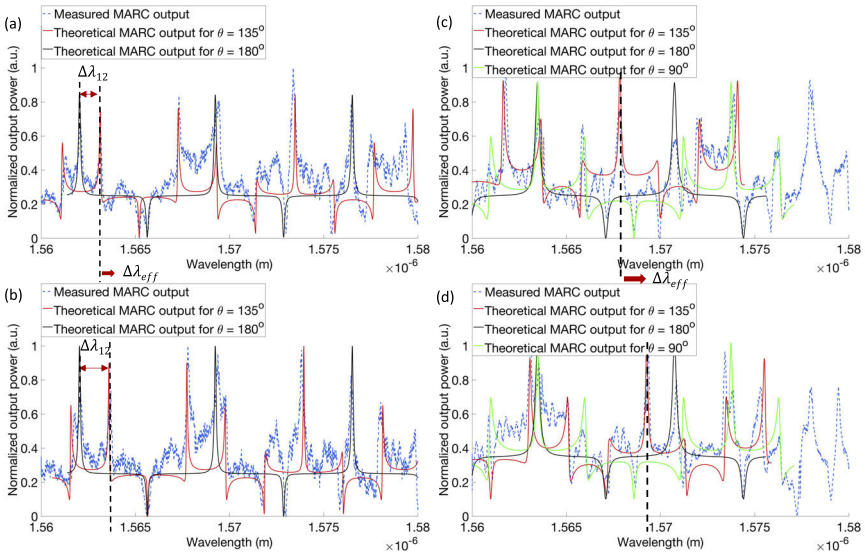


**Fig. 6.** Measured transmission response from multiplexed MARC sensors. (a) Multiplexed response from the MARC with two rings cladded with deionized water, (b) when ring with 135° angular separation was cladded with 6% saline solution, (c) Measured response from the MARC with 3 rings cladded with deionized water, (d) when ring with 135° angular separation was covered with 18% saline solution.

## 5. Discussion

MARC design presents a unique way to enhance the measurement range and improve multiplexing capability of a ring resonator based sensor. In the presented work, the measurement range was demonstrated only for a few configurations, and it can be further enhanced by tuning the angular separation. For multiplexing, the number of ring resonators in a MARC sensor can be further increased by improving the quality factor of individual ring resonators. Enhancement in the quality factor will reduce the intensity overlap between adjacent resonances and improve the distinguishability of response from different resonators multiplexed together. We expect that with further tuning of the angular separation and optimization of the quality factor, the measurement range and the multiplexing capability of MARC sensor will exceed the presented experimental results. Interrogation complexity will also increase with an increase in number of multiplexed sensors. Signal processing or pattern recognition techniques would be required to identify the spectral response from different sensors.

## 6. Conclusion

We have experimentally demonstrated a multiplexed MARC sensor with a large measurement range. For a MARC sensor with 45 $\mu$m ring radius, the measurement range was ~16.1 nm which is 8 times larger than for a standard ring resonator sensor. In contrast to the standard ring resonator sensor, large measurement range was obtained without affecting the intrinsic Q-factor of the ring resonator. In addition to the enhancement in the measurement range, the transmission response from MARC for a specific angular separation provides a unique spectral signature. These spectral signatures were experimentally utilized to demonstrate the multiplexing capability of the MARC sensor. The large measurement range and the multiplexing capability of the MARC sensor makes the sensor very suitable for high throughput sensing for numerous applications.

**Funding.** Norges Forskningsråd (248869/O70, 295864).

Optics EXPRESS

**Acknowledgments.** The Research Council of Norway is acknowledged for the support to the Lab-on-a-chip Biophotonic Sensor Platform for diagnostics, project number 248869/O70 and the Norwegian Micro- and Nano-Fabrication Facility, NorFab, project number 295864. The authors would like to thank, Jens Høvik, Prof. Dag Roar Hjelme and Dr. Jong Wook Noh from the Department of Electronic Systems, NTNU for fruitful discussions.

**Disclosures.** M.Y. and A.A. have applied for patent GB2004009.3 for optical sensing apparatus.

**Data availability.** Data underlying the results presented in this paper are not publicly available at this time but may be obtained from the authors upon reasonable request.

## References

1. H. M. Robison and R. C. Bailey, "A guide to quantitative biomarker assay development using whispering gallery mode biosensors," Curr. protocols chemical biology **9**(3), 158–173 (2017).
2. T. Claes, J. G. Molera, K. De Vos, E. Schacht, R. Baets, and P. Bienstman, "Label-free biosensing with a slot-waveguide-based ring resonator in silicon on insulator," IEEE Photonics J. **1**(3), 197–204 (2009).
3. K. De Vos, I. Bartolozzi, E. Schacht, P. Bienstman, and R. Baets, "Silicon-on-insulator microring resonator for sensitive and label-free biosensing," Opt. Express **15**(12), 7610–7615 (2007).
4. C. F. Carlborg, K. B. Gylfason, A. Kazmierczak, F. Dortu, M. J. Ba nuls Polo, A. Maquieira Catala, G. M. Kresbach, H. Sohlström, T. Moh, L. Vivien, J. Popplewell, G. Ronan, C. A. Barrios, G. Stemme, and W. van der Wijngaart, "A packaged optical slot-waveguide ring resonator sensor array for multiplex label-free assays in labs-on-chips," Lab Chip **10**(3), 281–290 (2010).
5. R. Heideman and P. Lambeck, "Remote opto-chemical sensing with extreme sensitivity: design, fabrication and performance of a pigtailed integrated optical phase-modulated mach–zehnder interferometer system," Sens. Actuators, B **61**(1-3), 100–127 (1999).
6. R. Heideman, R. Kooyman, and J. Greve, "Performance of a highly sensitive optical waveguide mach-zehnder interferometer immunosensor," Sens. Actuators, B **10**(3), 209–217 (1993).
7. P. Prabhathan, V. Murukeshan, Z. Jing, and P. V. Ramana, "Compact soi nanowire refractive index sensor using phase shifted bragg grating," Opt. Express **17**(17), 15330–15341 (2009).
8. E. Luan, H. Yun, M. Ma, D. M. Ratner, K. C. Cheung, and L. Chrostowski, "Label-free biosensing with a multi-box sub-wavelength phase-shifted bragg grating waveguide," Biomed. Opt. Express **10**(9), 4825–4838 (2019).
9. T. Claes, W. Bogaerts, and P. Bienstman, "Experimental characterization of a silicon photonic biosensor consisting of two cascaded ring resonators based on the vernier-effect and introduction of a curve fitting method for an improved detection limit," Opt. Express **18**(22), 22747–22761 (2010).
10. Y. Zhang, J. Zou, Z. Cao, and J.-J. He, "Temperature-insensitive waveguide sensor using a ring cascaded with a mach–zehnder interferometer," Opt. Lett. **44**(2), 299–302 (2019).
11. X. Jiang, Y. Chen, F. Yu, L. Tang, M. Li, and J.-J. He, "High-sensitivity optical biosensor based on cascaded mach–zehnder interferometer and ring resonator using vernier effect," Opt. Lett. **39**(22), 6363–6366 (2014).
12. W. Bogaerts, P. De Heyn, T. Van Vaerenbergh, K. De Vos, S. Kumar Selvaraja, T. Claes, P. Dumon, P. Bienstman, D. Van Thourhout, and R. Baets, "Silicon microring resonators," Laser Photonics Rev. **6**(1), 47–73 (2012).
13. A. L. Washburn, L. C. Gunn, and R. C. Bailey, "Label-free quantitation of a cancer biomarker in complex media using silicon photonic microring resonators," Anal. Chem. **81**(22), 9499–9506 (2009).
14. M. Yadav, J. W. Noh, D. R. Hjelme, and A. Aksnes, "Spectral shaping of ring resonator transmission response," Opt. Express **29**(3), 3764–3771 (2021).